Reciprocal Interactions of Hairpin-Shaped Vortices and a Boundary Layer

N.-S. Liu,* S. J. Shamroth,† and H. McDonald‡
Scientific Research Associates, Inc., Glastonbury, Connecticut 06033

The present effort simulates the flow dynamics resulting from hairpin-shaped vortices in a boundary layer through the solution of the time-dependent, three-dimensional, compressible Navier-Stokes equations. Two simulations have been carried out. In the first case, the initial condition contains only one imposed hairpin-shaped vortex. In the second case, there are two incipient vortices separated by a short distance in the streamwise direction. The results add to the detailed understanding of the dynamic role of hairpin vortices in the entrainment, production, and continual replenishment of wall turbulence, as well as the process of the interaction, intertwining, and eventual conglomeration of vortices in boundary layers.

Introduction

IT is now widely accepted that near-wall coherent structures play a major role in the production and transport of turbulence in turbulent boundary-layer flows. Although there are a number of different structural features in turbulent wall boundary layers,[1] there exists strong evidence that hairpin vortices are a basic and dominant structure.[2,3] Being the tractable part of wall turbulence, these organized structures may contain most of the essential physics of the turbulent boundary layers. Thus, better understanding of the dynamical significance of hairpin vortices in boundary layers is not only important to unveil the physics of turbulence per se, but it also holds the key to the management and control of turbulence, which is of significant technological importance.

The study of hairpin vortices in a fully turbulent environment is greatly complicated by the presence of randomness and a number of other coexisting structures. Nevertheless, a viable way to gain better understanding of their role in turbulence dynamics is to study the flow events stimulated by synthetically generated hairpin vortices in initially laminar boundary layers, as demonstrated by an experimental study of a continuous street of hairpin vortices generated in a laminar boundary layer,[4] and, most recently, an experimental study of single hairpin vortices in an initially laminar environment.[5] These experimental results indicate that, once hairpin vortices are present in the near-wall region of a shear flow, they can kinematically multiply themselves in the spanwise direction and dynamically generate secondary vortices in a region behind the primary vortex head and between the vortex legs. In addition, these flow structures lead to both velocity statistics and visualization patterns that display many characteristics of a turbulent boundary layer.

In the past, the most common theoretical approach for investigating the evolution of hairpin vortices was to conduct inviscid simulations based upon appropriate discretization of the Biot-Savart law. Consequently, these calculations cannot be carried out to the point where the viscous effects become important in the deformation or interaction of vortices. Furthermore, the Biot-Savart type of approach often neglects the effect of the vortical filament on the background flows.[6] In particular, the generation of new perturbation vorticity has not been considered. In fact, the neglect of the reciprocal interactions between a hairpin vortex and the background flow could greatly limit the validity of the results obtained from the Biot-Savart type of approach.[7] Nevertheless, inviscid simulation based on the Biot-Savart law has been a useful tool in gaining more insight into the kinematic features of the vortex deformation. Recently, it has been used to investigate the evolution of a hairpin vortex in a stagnant flow as well as in a shear flow.[8] Calculations for the evolution of a pair of interacting hairpin vortices in a shear flow also have been made. For understanding the dynamic role of hairpin vortices in wall turbulence, some progress has been made with simpler two-dimensional flows in establishing the effects of convected vortex motions on viscous flows near a wall.[9] It is argued that convected vortices will provoke eruptions of the near-wall fluid.

In addition, it has been theoretically demonstrated that the existence of a hierarchy of hairpin vortices is consistent with a logarithmic time-mean velocity profile,[10] and reasonable estimations of broadband turbulence intensity distributions could be obtained from this assumed hierarchy of hairpin vortices.[11] Such a hairpin vortex model of wall turbulence also has been extended to compressible flows.[12]

Several recent studies[13,14] suggest that many vortical structures in turbulent boundary layers are quite asymmetrical, and symmetrical hairpin-like vortices are relatively rare. Nevertheless, many important dynamical features of vortical structures in wall turbulence could be captured by studying the behavior of symmetrical vortices, as demonstrated by the aforementioned works and the results obtained under the present investigation.

The present effort investigates the flow dynamics stimulated by hairpin vortices in an initially laminar boundary layer through the direct solution of time-dependent, three-dimensional, compressible Navier-Stokes equations. The numerical procedure used in this effort is a temporal-spatial simulation. Two simulations have been carried out. In the first case, the initial condition contains only one imposed hairpin-shaped vortex. In the second case, there are two incipient vortices separated by a short distance in the streamwise direction. A detailed description of these simulations and the analyzed results can be found in Ref. 15. In the present paper, only a selected review of results elucidating the dynamic role of hairpin vortices in wall layers will be given.

Presented as Paper 90-0017 at the AIAA 28th Aerospace Sciences Meeting, Reno, NV, Jan. 8-11, 1990; received Feb. 20, 1990; revision received May 27, 1990; accepted for publication June 2, 1990.

*Senior Research Scientist; currently at NASA Lewis Research Center, Cleveland, OH 44135. Member AIAA.
†Vice President. Member AIAA.
‡President. Member AIAA.

Outline of Numerical Simulation

Governing Equations and Solution Procedure

The unsteady, three-dimensional, compressible Navier-Stokes equations, supplemented by an equation of state and together with the constant total temperature assumption, form the system governing the flows in the present effort. The total temperature assumption was made mainly to conserve computer run time and can be easily removed through inclusion of an energy equation. Solutions of the governing equations with low freestream Mach number, subject to prescribed initial condition and appropriate boundary conditions, are obtained by the consistently split linearized block implicit (LBI) technique.[16] Since the present numerical approach allows the specification of inflow-outflow as well as freestream conditions, it provides spatial-temporal simulations that describe the time evolution of spatial structures in a flow domain containing a boundary layer that is itself spatially changing.

The Incipient Hairpin-Shaped Vortex

The present study requires the specification of an initial flowfield that includes an incipient vortex structure. This field is based upon the following hairpin-vortex model, which is regarded here as the simplest conceptual model capturing the main features of hairpin vortices in turbulent boundary layers.

The model of the incipient hairpin vortices used in the present work to generate an initial flowfield consists of a spanwise array of vortices. The effective centerline of these vortices forms an array of interconnecting isosceles triangles that are periodic in the spanwise direction. Their wall images are included in order to maintain the attachment of these vortices to the rigid wall. A schematic of the present model is shown in Fig. 1, where h_i is the height of the ith array of hairpin vortices, λ_i the spanwise distance between the feet of the vortices, $\phi_i = \phi = 45$ deg the characteristic angle, and r_{oi} the radius of the effective core. The signature or the induced velocity is constructed with the aid of Biot-Savart law, supplemented by modifications that 1) account for the existence of a finite vortex core and 2) insure the satisfaction of no-slip conditions on the wall.

It is noted here that induced velocity field constructed by invoking the Biot-Savart law contributes to the solenoidal part of the total velocity of a compressible flow, as any vector can be resolved uniquely into an irrotational part and a solenoidal part.

Obviously, when the array contains a sufficiently large number of vortices, the induced field gives rise to periodic functions with spatial period λ_i. Therefore, the induced field due to such an array of vortices is completely described by the flowfield within the spanwise domain of any one of its members. The term "representative hairpin vortex" is used here to denote a vortex member arbitrarily chosen for constructing the flowfield information. It is noted here that, due to this initial arrangement of the incipient hairpin vortex and the use of a two-dimensional background flow, symmetrical conditions can be applied on the planes $z = -0.5\lambda_i$ and $z = 0$; i.e., the computational domain needs only to contain one leg of the representative hairpin vortex.

Flow Conditions and Parameters

The background flow is a zero-pressure-gradient laminar boundary-layer flow with a freestream Mach number of 0.4; i.e., it is a Blasius flow. The inflow section of the computational domain is located at a plane where $Re_{\delta^*} = 419$ and the outflow section is located at a plane where $Re_{\delta^*} = 576$, where Re_{δ^*} is the Reynolds number based on freestream velocity and the local displacement thickness. Thus, the computational domain contains both subcritical and supercritical growth regions, as defined by linear stability theory.

As for the imposed representative hairpin-like vortex, the initial configuration is such that the inclination angle is 45 deg toward the downstream direction, the height h is $0.5\delta_o$, and the spanwise spacing between the vortex feet is $2\delta_o$ where δ_o is the boundary-layer thickness at a streamwise location where $Re_{\delta^*} = 490$. The initial strength of the imposed vortex is chosen so that the maximum value of its induced velocity is 8.5% of the freestream velocity. The height and the maximum induced velocity of this imposed vortex are comparable to those experimentally generated[4] but the spanwise spacing differs by a factor of 4. The larger spanwise spacing between vortex legs is chosen to alleviate the demand of grid resolution in the numerical simulation. Although this represents a quantitative difference with some experimentally generated hairpin vortices, the qualitative behavior of the interaction should not be affected. Two simulations have been conducted. In the first case, only one representative hairpin-like vortex is imposed, with its legs attached to the wall at the location where $Re_{\delta^*} = 487$. In the second case, two representative vortices are imposed, the streamwise separation between them is 1.5 h. The trailing vortex is attached to the wall at $Re_{\delta^*} = 485$, and the leading vortex is attached to the wall at $Re_{\delta^*} = 491$.

The streamwise (i.e., x-direction) extent of the computational domain has a length of $33\delta_o$ and is resolved by 250 grid points. In the region originally containing the incipient hairpin vortices, the grid spacing Δx is uniform with $\Delta x = 0.1h$. Forty points are contained in this region and the total extent is $4h$. In neighboring regions, Δx is gradually increased from 0.1–$0.2h$ and is kept at a value of $0.2h$ for the rest of the streamwise distance. The vertical (i.e., y-direction) extent of the computational domain has a length of $5\delta_o$ covered by 55 grid points. The height of the incipient vortex is resolved with 20 grid points, with Δy varying smoothly from $\Delta y = 0.04h$ to $\Delta y = 0.1h$. Furthermore, the grid spacing in the region from $y = 1.07h$ to $y = 4.19h$ is essentially uniform with $\Delta y = 0.13h$. The spanwise (i.e., z direction) extent of the computational domain has a length of δ_o covered with 15 grid points. The grid spacing is uniform with $\Delta z = 0.143h$. A constant (dimensionless) $\Delta t = 0.004$ is used for the calculations. In terms of the wall unit, Δt^+ is approximately 0.12. The simulations have been carried out for a time span over which the head of the incipient vortex has traveled a distance of approximately $7h$. It is noted here that simulations with finer grid spacings and/or smaller time steps have not been performed to assess the accuracy of the present numerical results. Nevertheless, experiences suggest that the chosen grid sizes and time step should provide adequate spatial and temporal resolutions for the present simulations.

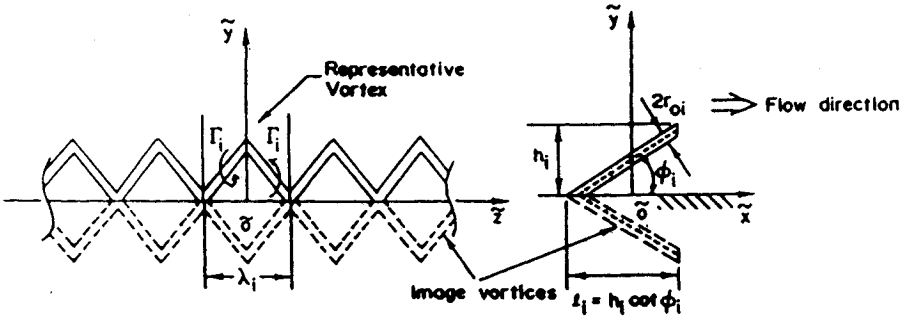

Fig. 1 A schematic of an array of hairpin vortices and the definition of a representative vortex.

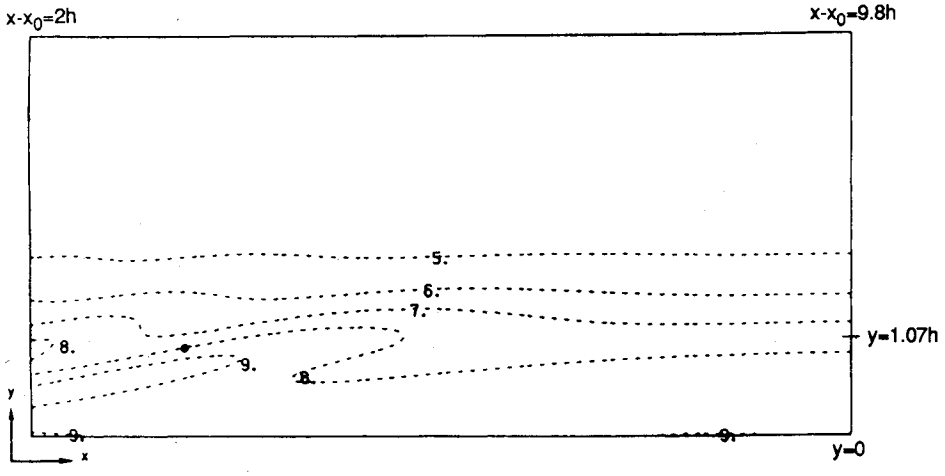

Fig. 2a Contours of spanwise vorticity Ω_z in the center plane: $t = 0.30$, $\Omega_{z,\min} = -34.082$.

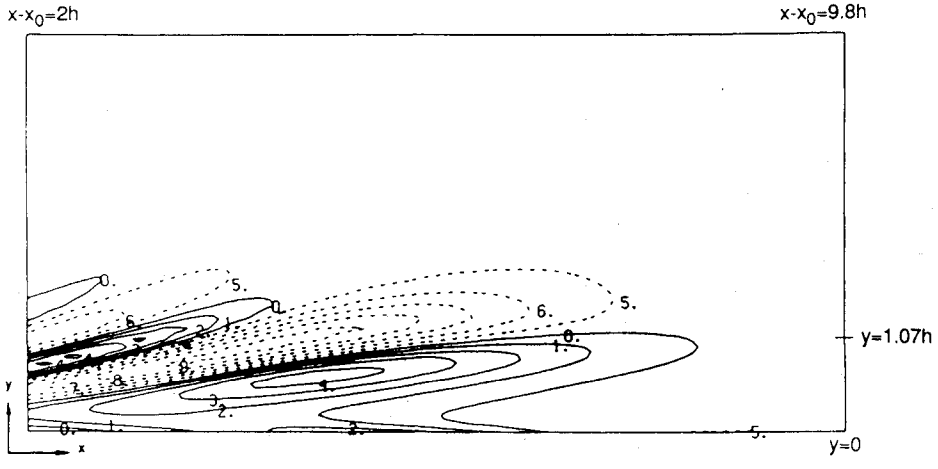

Fig. 2b Contours of induced spanwise vorticity Ω'_z in the center plane: $t = 0.30$, $\Omega'_{z,\min} = -6.974$, $\Omega'_{z,\max} = 4.970$.

Results

The present simulations yield results that are consistent with the generic features of hairpin-vortex kinematics and dynamics in shear layers.[4,5,8,17] For example, the kinematic deformation of the primary vortex is mainly through Biot-Savart induction. The vortex head rises through the layer and tends to become rounded. The legs are stretched and tend to move towards each other. From the point of view of dynamic interaction, as the head of the vortex passes by, it always impresses a region of adverse pressure gradient on the wall while its legs act as a transport vehicle to remove fluid from the wall. Secondary vortices are created behind the vortex head and between the vortex legs. In addition, three-dimensional vortex amalgamation contributes to the overall self-sustaining processes among hairpin vortices in proximity. Because of the complexities of the flow under consideration, it is very difficult to make quantitative comparisons with results reported by other investigators. It is further noted here that, in simulations and experiments with a single incipient hairpin vortex, this vortex can kinematically multiply itself into a spanwise array, while the present work deals with a preexisting, spatially periodic array of vortices. In the following, selected results are presented to elucidate the dynamic role of hairpin vortices in the production and continual replenishment of wall turbulence. A more detailed set of results are given in Ref. 15.

To illustrate the redistribution of spanwise vorticity (i.e., Ω_z) due to the presence of the hairpin vortex, the evolution of Ω_z in a region downstream of the incident vortex is shown in Fig. 2a, which is a contour plot in the center plane ($z = 0$). The dotted lines represent negative-valued contour lines, whereas the solid lines are positive-valued contour lines. Contour lines labeled 0–4 are associated with $f_{\max}$, the maximum value of the variable f, where f represents any plotted quantity. Labels of 0, 1, 2, 3, 4 represent 0.1, 0.3, 0.5, 0.7, $0.9 f_{\max}$, respectively, for $f_{\max} > 0$. Similarly labels 5, 6, 7, 8, 9 represent 0.1, 0.3, 0.5, 0.7, $0.9 f_{\min}$, respectively, for $f_{\min} < 0$. In the course of time, the pattern changes from initially laminate layers to significant undulations accompanied with scattered but highly vortical pockets, as shown in Fig. 2a. This phenomenon can be better understood by examining the behavior of induced vorticity Ω'_z defined as the difference between the instantaneous value and the background value. It can be seen that, as the original hairpin vortex ($\Omega'_z < 0$) convects past the wall, it induces vorticity of opposite sign ($\Omega'_z > 0$) in the near-wall region due to the no-slip conditions at the wall as shown in Fig. 2b. As a result, the background vorticity experiences a depletion in the near-wall region as shown in Fig. 2a. This, combined with the presence of the advected hairpin vortex and other vorticity depletion/intensification regions, leads to undulations in spanwise vorticity of the composite flow.

The "dot" in Fig. 2 represents a probe position at which time records of various quantities have been obtained. The time history of the spanwise vorticity Ω_z is shown in Fig. 3a. $Q(\Omega_z)$ relates to the production of Ω_z due to 1) the straining of the total vorticity and 2) the compressibility of the flow. Its temporal behavior is given in Fig. 3b. The transfer of Ω_z due to viscosity is denoted by $DF(\Omega_z)$, and it is shown in Fig. 3c. It is observed that, over this time period, $Q(\Omega_z)$ and $DF(\Omega_z)$ are out of phase and the variation of Ω_z is controlled by $Q(\Omega_z)$. It is also noted here that $Q(\Omega_z)$ is mainly due to the stretching by the normal strain e_{zz}, the contributions due to shearing strain are not yet significant.

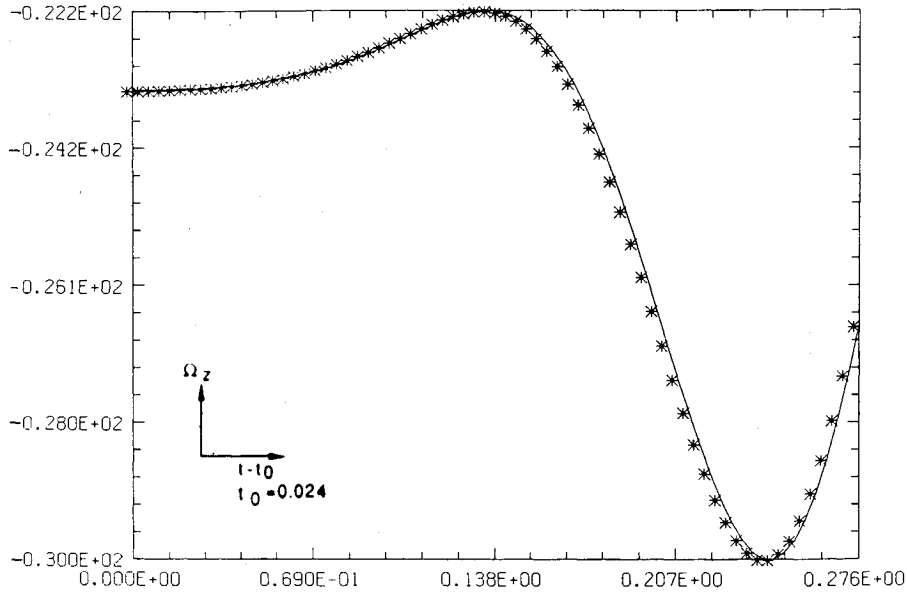

Fig. 3a Time record of spanwise vorticity Ω_z.

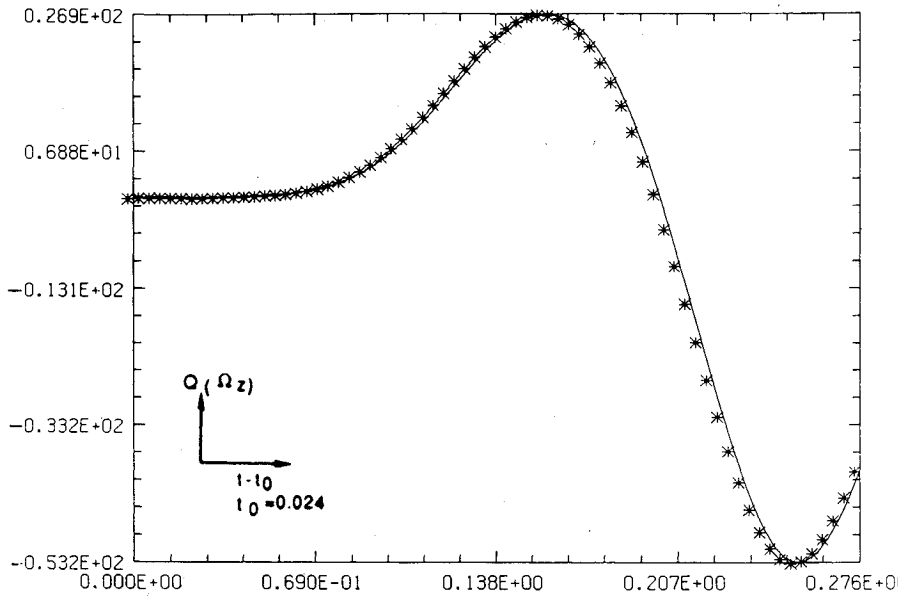

Fig. 3b Time record of the production of Ω_z, i.e., $Q(\Omega_z)$.

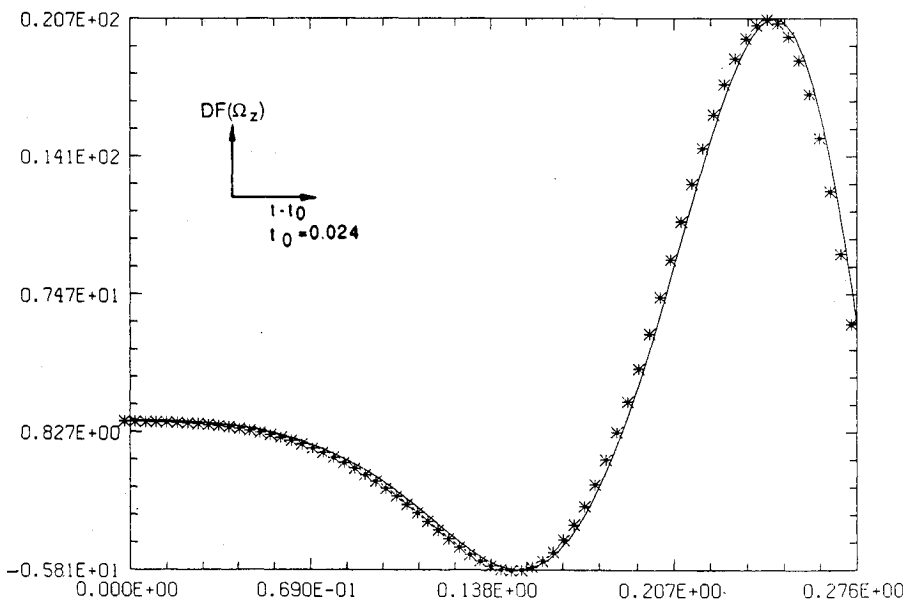

Fig. 3c Time record of the viscous diffusion of Ω_z, i.e., $DF(\Omega_z)$.

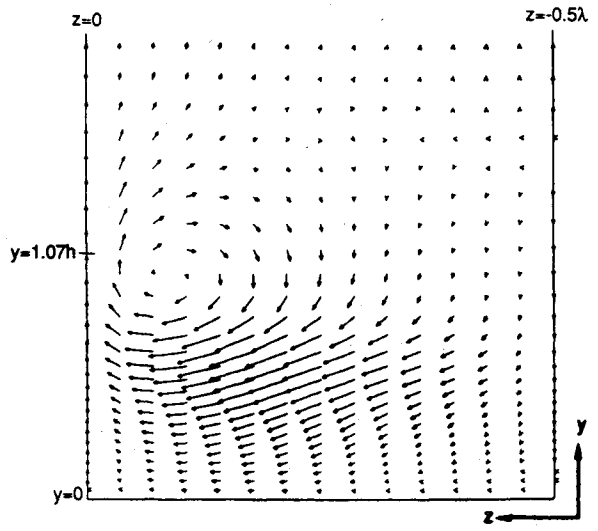

Fig. 4a Crossflow velocity field (v,w): $t = 0.10$, $x - x_o = 1.7h$, $q_{max} = 0.022$.

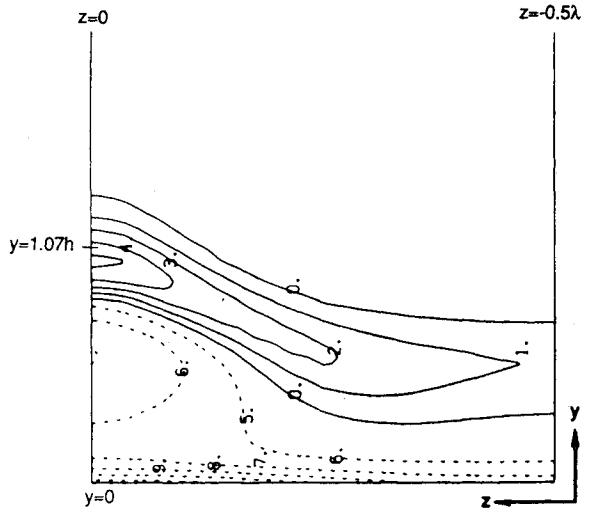

Fig. 5a Contours of $\phi' \times 10$ in a crossflow plane: $t = 0.10$, $x - x_o = 1.7h$, $\phi'_{min} = -0.133$, $\phi'_{max} = 0.085$.

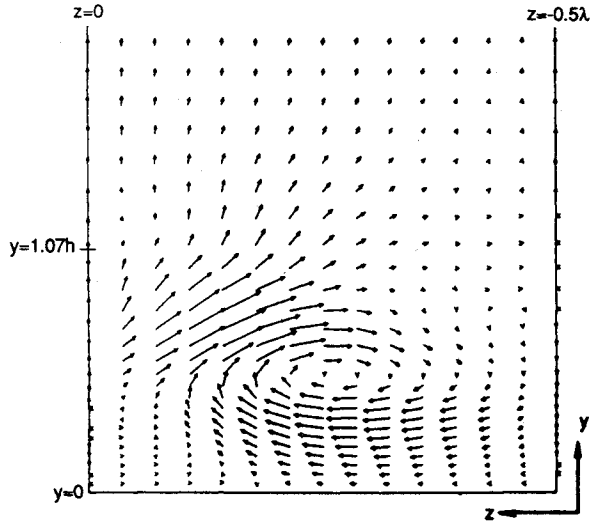

Fig. 4b Crossflow velocity field (v,w): $t = 0.18$, $x - x_o = 1.7h$, $q_{max} = 0.027$.

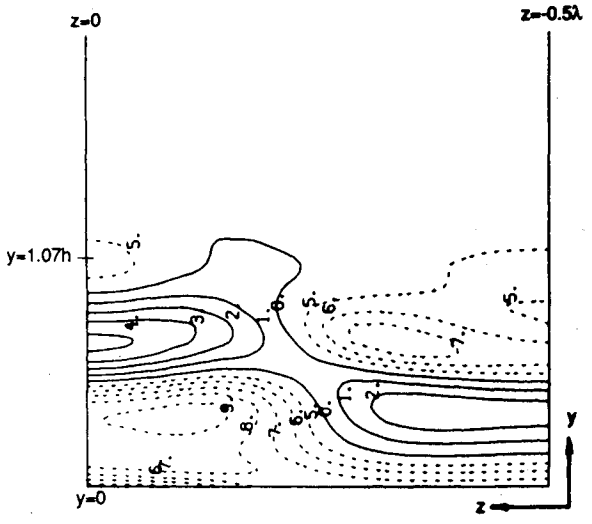

Fig. 5b Contours of $\phi' \times 10$ in a crossflow plane: $t = 0.18$, $x - x_o = 1.7h$, $\phi'_{min} = -0.077$, $\phi'_{max} = 0.131$.

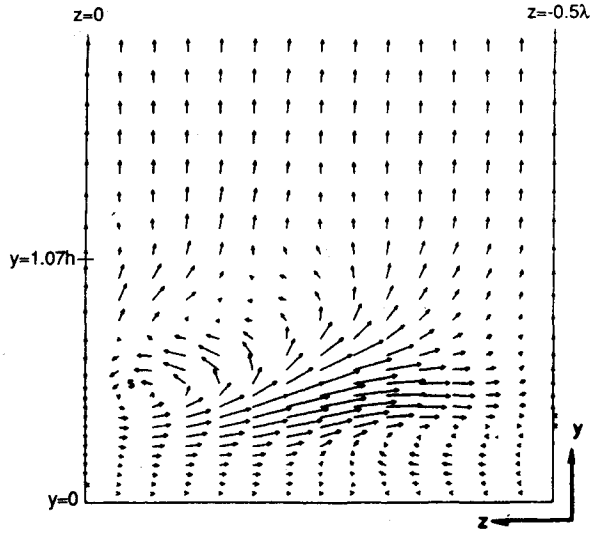

Fig. 4c Crossflow velocity field (v,w): $t = 0.30$, $x - x_o = 1.7h$, $q_{max} = 0.015$.

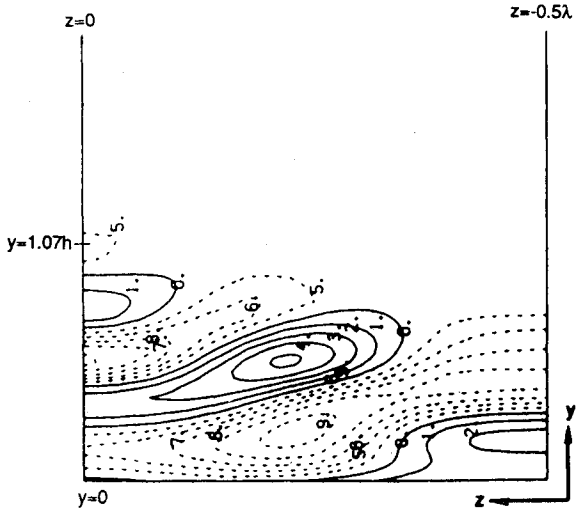

Fig. 5c Contours of $\phi' \times 10$ in a crossflow plane: $t = 0.30$, $x - x_o = 1.7h$, $\phi'_{min} = -0.074$, $\phi'_{max} = 0.122$.

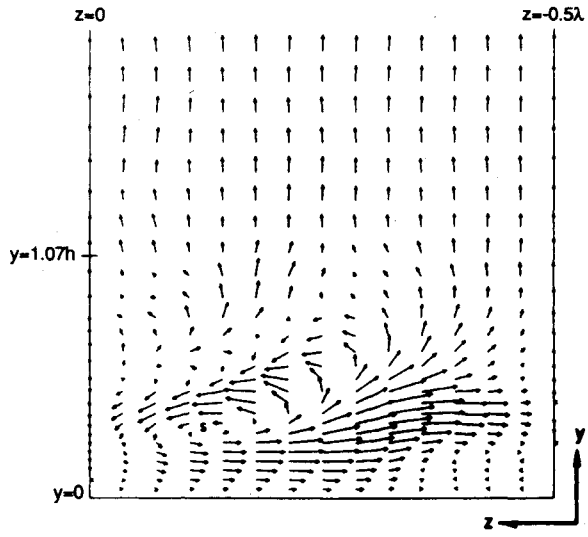

Fig. 6a Crossflow velocity field (v,w): $x - x_o = 0.9h$, $t = 0.30$, $q_{max} = 0.011$.

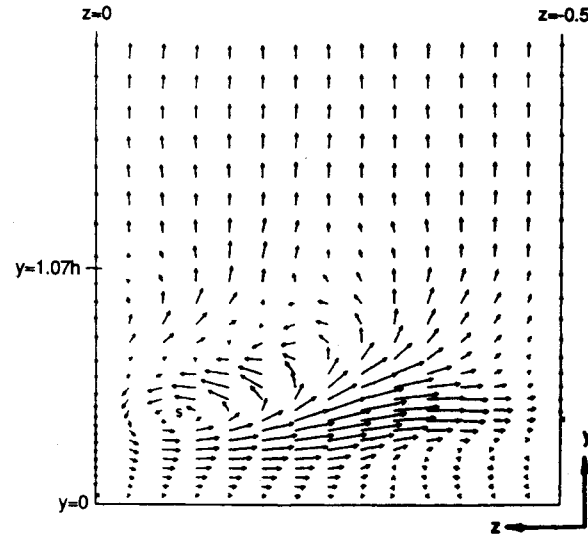

Fig. 6b Crossflow velocity field (v,w): $x - x_o = 1.3h$, $t = 0.30$, $q_{max} = 0.013$.

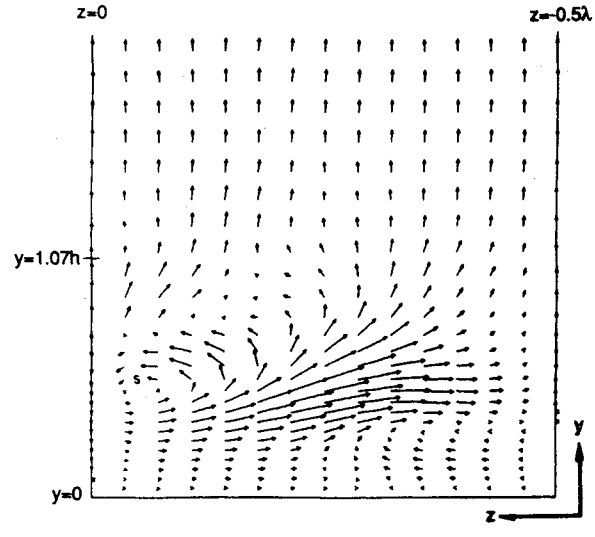

Fig. 6c Crossflow velocity field (v,w): $x - x_o = 1.7h$, $t = 0.30$, $q_{max} = 0.015$.

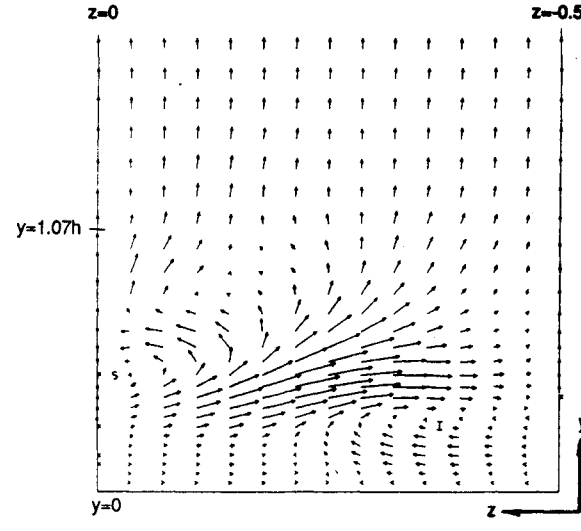

Fig. 6d Crossflow velocity field (v,w): $x - x_o = 2.0h$, $t = 0.30$, $q_{max} = 0.017$.

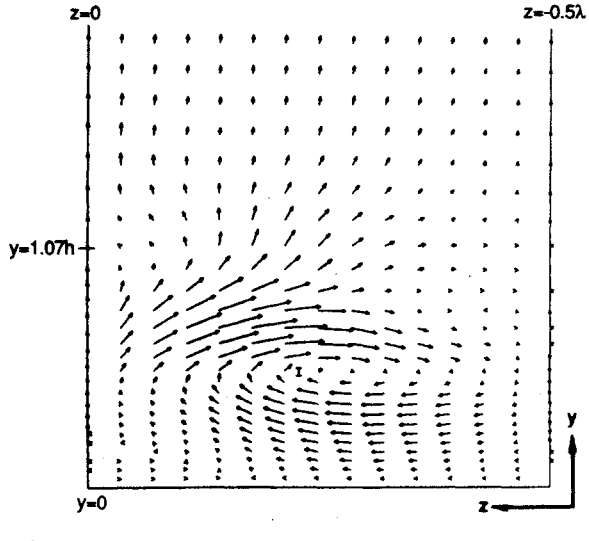

Fig. 6e Crossflow velocity field (v,w): $x - x_o = 3.6h$, $t = 0.30$, $q_{max} = 0.022$.

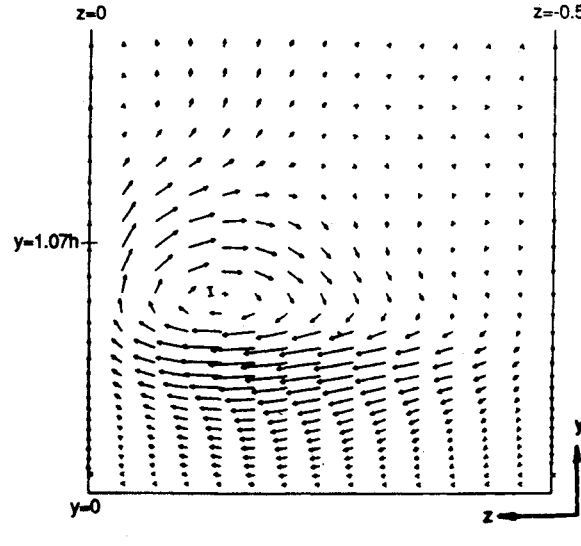

Fig. 6f Crossflow velocity field (v,w): $x - x_o = 5.2h$, $t = 0.30$, $q_{max} = 0.017$.

In the following, the temporal development of the flow in a fixed y-z plane will be used to illustrate the kinematic and dynamic aspects of the events stimulated by the reciprocal interactions between the initially imposed vortex and the background flow. This plane is located at $x - x_o = 1.7h$, where x_o is the streamwise coordinate of the tip of the initially imposed vortex. The view looks upstream into the main flow. Figure 4a–c presents the development of the crossflow velocity field in the course of time, where q_{max} is the instantaneous magnitude of the maximum crossflow velocity. The passage of the primary vortex and the subsequent emergence of a counter-revolving secondary vortex near the lower part of the center plane (Fig. 4c) are the most salient features. The secondary vortex is denoted in Fig. 4c by "S." Figure 4a is at time $t = 0.10$. This is before any significant interaction occurs and the flow pattern is clearly due to the initial vortex. The vortex leg cuts the fixed y-z plane at a location near the centerline. Figure 4b shows the pattern at a later time. The vortex has moved downstream and the portion of the leg of the initial vortex is at a spanwise location further removed from the centerline. In addition, a counter-rotating vortex is becoming evident near the centerline; this is more clearly evident in Fig. 4c. The existence of such a secondary vortex will be further demonstrated in Fig. 6. At this point, some other results are described. It is observed that the primary vortex consistently occupies one of the low pressure regions and the emergence of a secondary vortex is closely associated with the appearance of a high-pressure region in the immediate neighborhood of a low-pressure region. The passage of the primary vortex induces very thin shear layers across which large gradients of the shear stress vector in the y-z plane occur. Furthermore, the secondary vortex is in the close proximity of some of these thin shear layers. It has been suggested that such secondary vortical structures are generated owing to the roll-up of the high-shear layer that develops between the lifted-up low momentum, wall-layer fluid, and the higher-momentum outer-boundary-layer flow.[4]

The dissipation of energy per unit mass ϕ characterizes the rate at which the total available energy is being lost by viscous dissipation. Thus, it would be interesting to examine the changes of this quantity induced by the presence of the hairpin-like vortex. Figure 5a–c presents the increase/decrease of the energy dissipation rate over a period of time. The solid contour lines represent an increase, whereas the dotted lines represent a decrease. As the head of the primary vortex is approaching this particular y-z plane, there is an increase of energy dissipation rate (i.e., $\phi' > 0$) in the region closer to the head. However, the rate of energy dissipation is appreciably decreased in the near-wall region. As the primary vortex passes through this plane, patterns of ϕ' do change, but the essential features are the alternative increase and decrease of dissipation rate around the periphery of its core and the appearance of a secondary vortex with its core residing in a region in which the viscous dissipation rate is largely reduced.

Figure 6a–f describes the spatial distribution of the crossflow over an extended streamwise domain. These plots are crossflow velocity fields in various y-z planes. The orientation of these figures is with respect to a viewer positioned in the downstream region of these planes while looking toward the upstream direction. The revolving flow patterns associated with the initially imposed hairpin vortex are denoted by "I." These flow patterns are taken at $t = 0.30$ at which time the primary vortex has convected downstream from its initial location.

The flow plane shown in Fig. 6a is located well upstream of the primary vortex, and the flow shown here is that due to the secondary vortex induced by the primary vortex. The location of this secondary vortex is denoted by "S." As previously discussed, this secondary vortex appears upstream of the primary vortex and is between the primary vortex legs. Figure 6b–f shows the crossflow field at successively downstream locations. In Figure 6a–d, the secondary vortex cuts the plane at successively higher and more inboard locations. The primary vortex with little influence from the secondary vortex is shown in Fig. 6f. The advection, stretching, and deformation of this primary vortex are clearly demonstrated in these plots. As shown in Fig. 6e and 6f, the original vortex remains quite coherent as it is convected downstream. Although not shown here, in regions which initially were occupied by the incipient vortex, the crossflow patterns now become somewhat incoherent and reminiscent of turbulent flow patterns.[15] Therefore, Fig. 6 and other related results show convection of the original vortex, generation of a secondary vortex of opposite revolving direction behind the primary vortex head and between its legs, and generation of a noncoherent region in the far wake of the primary vortex.

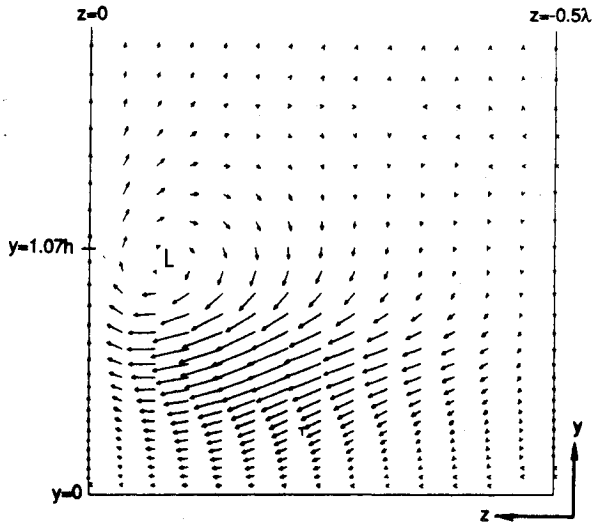

Fig. 7a Crossflow velocity field (v,w): $x - x_o = 2.1h$, $t = 0.10$, $q_{max} = 0.020$.

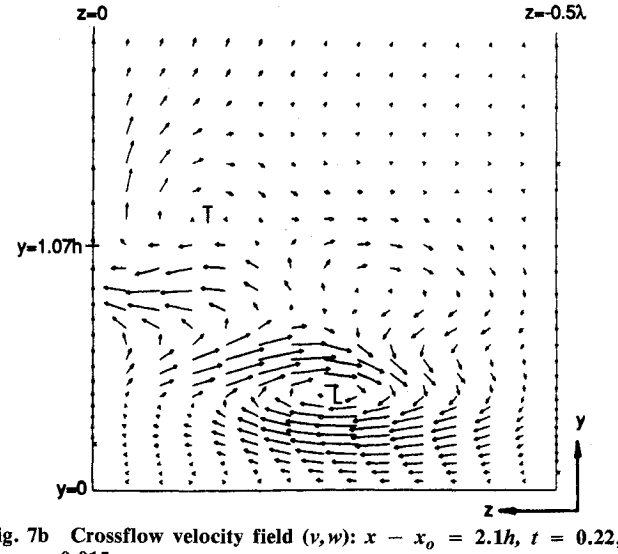

Fig. 7b Crossflow velocity field (v,w): $x - x_o = 2.1h$, $t = 0.22$, $q_{max} = 0.015$.

The following results are obtained from a simulation where its initial condition consists of two "representative" hairpin-shaped vortices separated with a streamwise distance of $1.5h$. In brief, the results demonstrate that these two vortices intertwine with each other and eventually merge into a single but somewhat reinforced vortex. This is illustrated in Fig. 7a and 7b. These figures depict the temporal development of the crossflow in a plane normal to the streamwise direction and located at $x - x_o = 2.1h$, where x_o is the streamwise coordinate of the tip of the incipient "leading" vortex. Figure 7a

indicates the passage of the leading vortex through this cross-flow plane, and Fig. 7b demonstrates that the head of the trailing vortex is interacting and intertwining with the leg of the leading vortex. In these figures, "L" indicates the leading vortex and "T" indicates the trailing vortex. More detailed results of vortex-vortex-wall layer interactions will be reported in a separate paper.

Conclusions

The present effort simulates the flow dynamics stimulated by hairpin vortices in a boundary layer through the direct solution of time-dependent, three-dimensional, compressible Navier-Stokes equations. These simulations show that, as a hairpin vortex passes over a wall, it induces opposite-sign vorticity at the wall, thus the overall spanwise vorticity in the near-wall region is being depleted. Furthermore, the energy dissipation in this region is also being decreased. The reciprocal interactions of primary vortices and background shear flow always generate secondary vortices, some of them are hairpin-shaped. It is observed that an advecting hairpin vortex leaves behind in its wake an unsteady three-dimensional strain field, which will then create vorticity fluctuations through volumetric dilatation and straining of currently active vorticity components. In accordance with the Biot-Savart law, these newly created vorticity fluctuations are associated with the solenoidal part of the new velocity fluctuations both in the near and far-field regions. When two hairpin vortices are separated by a short streamwise distance, they will intertwine and eventually coalesce into a reinforced hairpin vortex. This amalgamation contributes to the overall self-sustaining processes among hairpin vortices. Obviously, this study of coherent structures in boundary layers is by no means complete. There is a variety of research directions that could be pursued in the future. For example, the modulation of the development of hairpin vortices through outer disturbances, the effects of pressure gradients, and the behavior of vortical structures in highly compressible flows are possible new research areas.

Acknowledgments

The authors acknowledge the support of the U.S. Air Force Office of Scientific Research under Contract F49620-86-C-0028. James McMichaels was the contract monitor.

References

[1]Kline, S. J., "Quasicoherent Structures in the Turbulent Boundary Layer: Pt. 1. Status Report on a Community-Wide Summary of the Data," Zoran P. Zaric Memorial International Seminar on Near-Wall Turbulence, Dubrovnik, Yugoslavia, May 1988.

[2]Head, M. R., and Bandyophadyay, P., "New Aspects of Turbulent Boundary-Layer Structure," *Journal of Fluid Mechanics,* Vol. 107, June 1981, pp. 297–337.

[3]Moin, P., and Kim, J., "The Structure of the Vorticity Field in Turbulent Channel Flow: Pt. 1. Analysis of Instantaneous Fields and Statistical Correlations," *Journal of Fluid Mechanics,* Vol. 155, June 1985, pp. 441–464.

[4]Acarlar, M. S., and Smith, C. R., "A Study of Hairpin Vortices in a Laminar Boundary Layer: Pt. 1. Hairpin Vortices Generated by Hemisphere Protuberances; and Pt. 2. Hairpin Vortices Generated by Fluid Injection," *Journal of Fluid Mechanics,* Vol. 175, Feb. 1987, p. 1, 43.

[5]Haji-Hairdari, A., Taylor, B., and Smith, C., "The Generation and Growth of Single Hairpin Vortices," AIAA Paper 89-0964, March 1989.

[6]Aref, H., and Flinchem, E. P., "Dynamics of a Vortex Filament in a Shear Flow," *Journal of Fluid Mechanics,* Vol. 148, Nov. 1984, pp. 447–497.

[7]Moin, P., Leonard, A., and Kim, J., "Evolution of a Curved Vortex Filament into a Vortex Ring," *Physics of Fluids,* Vol. 29, April 1986, pp. 955–963.

[8]Hon, T. L., and Walker, J. D. A., "Evolution of Hairpin Vortices in a Shear Flow," NASA TM-100858, ICOMP-88-9, July 1988.

[9]Ersoy, S., and Walker, J. D. A., "Flow Induced at a Wall by a Vortex Pair," *AIAA Journal,* Vol. 24, No. 10, 1986, p. 1597.

[10]Perry, A. E., and Chong, M. S., "The Mechanism of Wall Turbulence," *Journal of Fluid Mechanics,* Vol. 119, June 1982, pp. 173–217.

[11]Perry A. E., Henbest, S. M., and Chong, M. S., "A Theoretical and Experimental Study of Wall Turbulence," *Journal of Fluid Mechanics,* Vol. 165, April 1986, pp. 163–199.

[12]Fernando, E. M., and Smits, A. J., "The Kinematics of Simple Vortex-Loop Arrays," AIAA Paper 88-3657, July 1988.

[13]Robinson, S. K., Skline, S. J., and Spalart, P. R., "Quasicoherent Structures in the Turbulent Boundary Layer: Pt. II. Verification and New Information from a Numerically Simulated Flat-Plate Layer," Zoran P. Zaric Memorial International Seminar on Near-Wall Turbulence, 1988.

[14]Guezennec, Y. G., Piomelli, U., and Kim, J., "Conditionally Averaged Structures in Wall-Bounded Turbulent Flows," *Studying Turbulence Using Numerical Simulation Data Bases,* Ames/Stanford CTR-S87, NASA Ames Research Center, 1989, p. 263.

[15]Liu, N. S., Shamroth, S. J., and McDonald, H., "Reciprocal Interactions of Hairpin-Shaped Vortices and a Boundary Layer," SRA Rept. R88-910016-F, Scientific Research Assoc. Inc., 1988.

[16]Briley, W. R., and McDonald, H., "On the Structure and Use of Linearized Block Implicit Schemes," *Journal of Computational Physics,* Vol. 34, No. 1, 1980, pp. 54–72.

[17]Smith, C. R., Walker, J. D. A., Haidari, A. H., and Taylor, B. K., "Hairpin Vortices in Turbulent Boundary Layers: The Implications for Reducing Surface Drag," *2nd UITAM Symposium on Structure of Turbulence and Drag Reduction,* edited by A. Gyr, Springer-Verlag, 1989.